Piezo-phototronic Effect Enhanced Visible and Ultraviolet Photodetection Using a ZnO–CdS Core–Shell Micro/nanowire

Fang Zhang,[†,‡] Yong Ding,[†] Yan Zhang,[†] Xiaoling Zhang,[‡] and Zhong Lin Wang[†,§,*]

[†]School of Material Science and Engineering, Georgia Institute of Technology, Atlanta, Georgia 30332-0245, United States, [‡]Key Laboratory of Cluster Science of Ministry of Education, School of Chemistry, Beijing Institute of Technology, Beijing 100081, China, and [§]Beijing Institute of Nanoenergy and Nanosystems, Chinese Academy of Sciences, Beijing, China

ABSTRACT

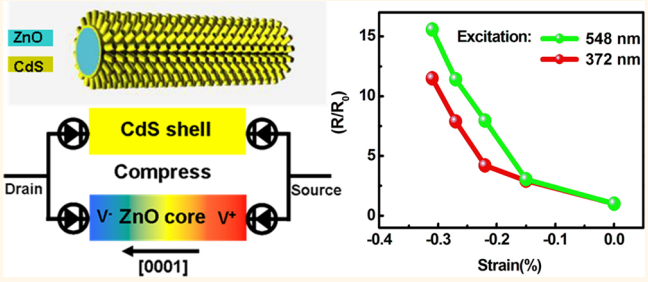

The piezo-phototronic effect is about the use of the piezoelectric potential created inside some materials for enhancing the charge carrier generation or separation at the metal–semiconductor contact or *pn* junction. In this paper, we demonstrate the impact of the piezo-phototronic effect on the photon sensitivity for a ZnO–CdS core–shell micro/nanowire based visible and UV sensor. CdS nanowire arrays were grown on the surface of a ZnO micro/nanowire to form a ZnO–CdS core–shell nanostructure by a facile hydrothermal method. With the two ends of a ZnO–CdS wire bonded on a polymer substrate, a flexible photodetector was fabricated, which is sensitive simultaneously to both green light (548 nm) and UV light (372 nm). Furthermore, the performance of the photon sensor is much enhanced by the strain-induced piezopotential in the ZnO core through modulation of the Schottky barrier heights at the source and drain contacts. This work demonstrates a new application of the piezotronic effect in photon detectors.

KEYWORDS: ZnO–CdS core–shell micro/nanowire · Schottky contact · piezopotential · photodetector · piezo-phototronic effect

One-dimensional semiconductor nanostructures are considered as the most sensitive and fast responsive materials for photon sensors due to their large surface-to-volume ratio and direct pathway for charge transport.[1−3] A variety of semiconductor nanowires (NWs) and nanobelts have been developed, such as group II–VI compounds ZnO (<3.37 eV, 370 nm) and ZnS (<3.77 eV, 335 nm) as the typical active materials for UV light and CdS (<2.40 eV, 516 nm) and CdSe (<1.74 eV, 712 nm) for visible light.[4−7] However, pure semiconductor NWs cannot absorb wavelengths below their band gap, which limits their wide-spectral sensitivity in standard devices, such as for visible/ultraviolet (UV) light imaging, memory storage or switches. Herein we report the performance of a single ZnO–CdS core–shell micro/nanowire based photodetector, which shows an excellent sensitivity and response from 372 to 548 nm. This is one of the most effective heterostructure-based multiband photodetectors for simultaneously detecting visible and UV light illumination.[8]

Moreover, the performance of such a photon sensor has been largely enhanced with the use of piezo-phototronic effect. The wurtzite structured ZnO NW exhibits high polarization performance. A piezoelectric potential (piezopotential) is created in the nanowire by applying a stress.[9] Recently, by the coupling of piezoelectric, optical, and semiconducting properties, the performance of photodetector based on a single ZnO wire has been improved, which is referred to as the piezo-phototronic effect.[10,11] The physical mechanism of this effect is to tune the charge transport/separation/recombination process at NW–electrode contacts by using strain induced piezoelectric field in the wire.[12] In our work, based on the unique crystalline structure of the ZnO–CdS core–shell wire, the performance of the photodetector can be further enhanced by strain induced piezopotential in the ZnO core through modulation of the Schottky barrier heights (SBHs) at the source and drain contacts. This result provides

* Address correspondence to zlwang@gatech.edu.

Received for review August 7, 2012 and accepted September 28, 2012.

Published online September 28, 2012
10.1021/nn3035765

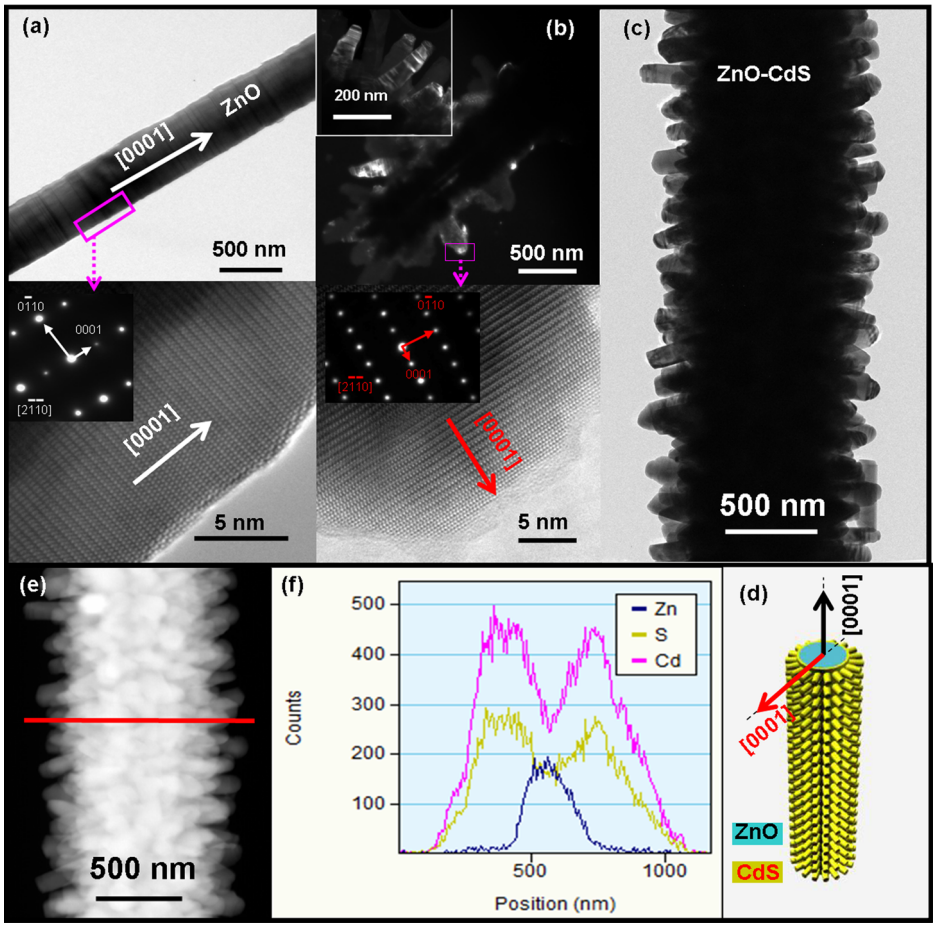

Figure 1. (a) Low-magnification TEM image of a ZnO nanowire, HRTEM image, and SAED pattern taken from the marked edge. (b) Dark-field TEM image of a ZnO–CdS nanowire, HRTEM image, and SAED pattern taken from the marked tip of a CdS nanowire. (c) Low-magnification TEM image of a ZnO–CdS wire. (d) Three-dimensional structure model of a ZnO–CdS core–shell wire, showing the structure relationship between ZnO wire core and CdS nanowire array shell. (e) STEM image of a ZnO–CdS nanowire. (f) The corresponding EDS elemental profile of Cd, S, and Zn along the red line in panel e.

a new method to optimize the performance of multifunction nanomaterials by introducing a piezo-phototronic effect.

RESULTS AND DISCUSSION

ZnO micro/nanowires were grown by thermal evaporation described in the previous literature.[13] Figure 1a is a low-magnification transmission electron microscopy (TEM) image, showing the details of a single ZnO NW. A high-resolution transmission electron microscopy (HRTEM) image and the corresponding select area electron diffraction (SAED) pattern taken from the edge of ZnO NW are presented, indicating that the ZnO wire is structurally uniform and single crystalline with length direction along the *c*-axis. Figure 1b displays a dark-field (DF) TEM image of a single ZnO–CdS NW; the inset is the magnified DF image of the CdS NW array with diameters of ~100 nm and lengths of ~500 nm, and the line-like contrasts are ascribed to stacking faults normal to the length axis. To further verify the crystalline structure of the CdS NWs, a high-resolution image and SAED pattern were taken at the marked tip region of a CdS NW, indicating that the CdS NW grows along the *c*-axis and the lattice fringes can be assigned to (0001). Figure 1c is a low-magnification TEM image of CdS NW array grown on the ZnO NW after hydrothermal reaction, showing the entire surface of the ZnO NW is uniformly covered by CdS NW array. A three-dimensional schematic configuration of a single ZnO–CdS wire in Figure 1d exhibits the oriented growth of CdS NW array toward outside on the surface of ZnO wire at the normal direction. To confirm the core–shell heterostructure, a more detailed investigation was conducted using field-emission transmission electron microscopy (FE-TEM). Figure 1e is a bright-field (BF) and scanning transmission electron microscopy annular dark field (ADF) image of an individual ZnO–CdS NW. An energy dispersive X-ray (EDX) line scan profile across the entire NW along the red line is presented in Figure 1f, which clearly demonstrates that Cd and S are distributed at the shell while the Zn located at the core.

An individual ZnO–CdS micro/nanowire-based photodetector was then constructed by a standard

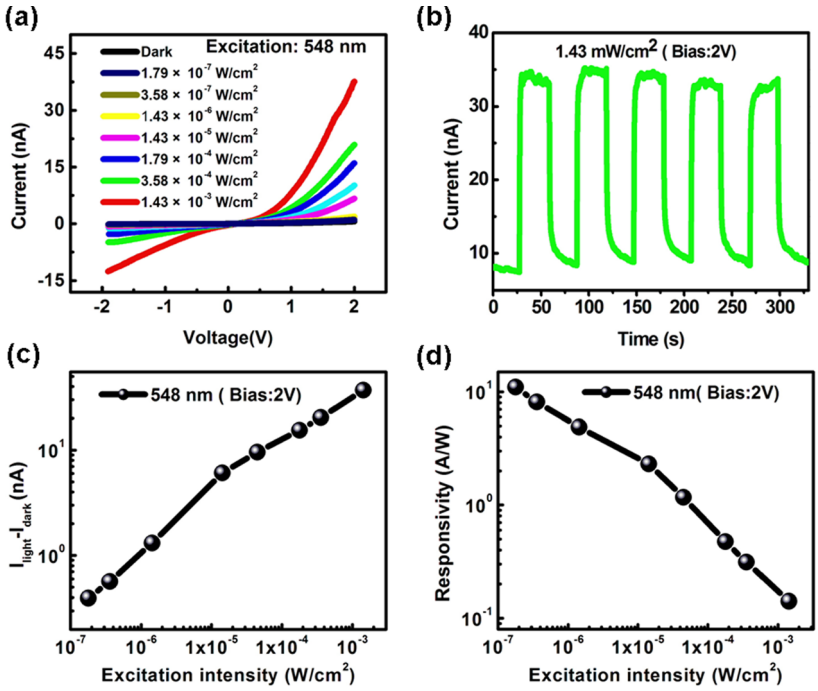

Figure 2. (a) Typical *I*–*V* characteristics of single ZnO–CdS wire-based device, excited by green light centered at 548 nm. (b) Repeatable response of a single ZnO–CdS wire-based device, excited by green light centered at 548 nm (1.43 mW/cm^2) (c) Absolute photocurrent of a single ZnO–CdS wire-based device measured as a function of the excitation intensity. (d) The derived photon responsivity relative to excitation intensity on the ZnO–CdS wire.

procedure (see the Experimental Section). The schematic structure and optical image of the photodetector are given in Supporting Information, Figure S1a,b showing the measurement setup. First, the performance of a single ZnO–CdS wire photodetector (device #1) under green light illumination (λ = 548 nm) is summarized. Figure 2a shows some typical *I*–*V* characteristics of the ZnO–CdS wire in the dark and under illumination at different light intensities from 1.79 × 10^{-7} W/cm^2 to 1.43 × 10^{-3} W/cm^2. Significantly, the absolute current increased from 0.6 nA (dark current) to 10.2 nA (4.48 × 10^{-5} W/cm^2) and further to 37.6 nA (1.43 × 10^{-3} W/cm^2) at an applied voltage of 2 V. Figure 2b illustrates the measured current response of a single ZnO–CdS wire based photodetector under 548 nm light illumination at a bias of 2.0 V. With the light irradiation off and on, the current of the device exhibits two distinct states, including a low-current state of 8.1 nA (which could reduce to 0.6 nA after 2 h) in the dark and a high-current state of 34.6 nA under light illumination. The current increases very sharply from one state to another state, with a response speed faster than 0.5 s. The excellent photocurrent reproducibility and stability indicate that the developed ZnO–CdS wire is a great candidate for applications in visible light detection.

Additionally, the intensity dependences of photocurrents ($I_{light} - I_{dark}$) are plotted in Figure 2c. As we can see, the photocurrent increased with the optical power and showed no saturation at high power levels, offering a large dynamic range from 10^{-7} to 10^{-3} W/cm^2. The sensitivity defined as ($I_{light} - I_{dark}$)/I_{dark} was found to be 6 × 10^3% (1.43 × 10^{-3} W/cm^2), which is about 10^3 times higher than CdS nanoribbon (550 nm, <5%) and 6 times higher than the aligned networks of CdS NWs on SiO_2 substrates.[14,15] Although the reason for this remarkable enhancement is not quite clear, we propose that it may be understood from the nanostructure of the CdS shell and band energy alignment of the ZnO–CdS wire. Generally, one-dimensional nanostructure arrays have the advantage of low reflectance due to light scattering and trapping, endowing them with superior optical absorption compared with a one-dimensional nanostructure.[16,17] Therefore, the CdS NW array grown on a ZnO wire is more efficient in generating a higher photocurrent, and thus increases the sensitivity of the photodetector. On the other hand, a type-II heterostructure with a staggered alignment at the heterjunction in the ZnO–CdS wire facilitates the spatial separation of the photon-generated carriers and can decrease the recombination of the electron–hole pairs, therefore significantly increasing the photocurrent and sensitivity of the device.[18,19] Such an enhancement effect has also been observed in ZnO/ZnS biaxial nanobelts.[20]

Moreover, the responsivity (*R*) is also a critical parameter to determine the capability of a photodetector.[21] The total responsivity of the photodetector *R* is defined as

$$R = \frac{I_{ph}}{P_{ill}} = \frac{\eta_{ext} q}{h\nu} \Gamma_G \quad (1)$$

$$P_{ill} = I_{ill} dl \quad (2)$$

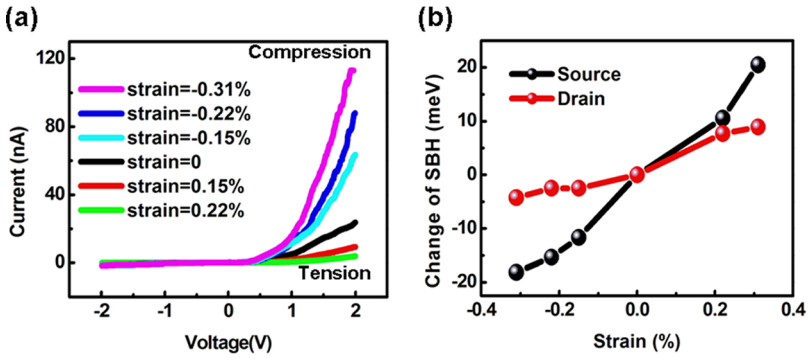

Figure 3. (a) Typical *I*−*V* characteristics of a single ZnO−CdS wire-based device under different compressive and tensile strains, excited by green light centered at 548 nm (1.43 mW/cm^2). (b) The derived change in SBH as a function of stain using the thermionic emission−diffusion model. Black curve and red curve are the SBH change for source contact and drain contact at a source−drain bias of *V* = 2 and −2 V, respectively.

where R is the responsivity, I_{ph} is the photocurrent, P_{ill} is the illumination power on the photodetector, η_{ext} is the external quantum efficiency (EQE), q is the electronic charge, h is Planck's constant, ν is the frequency of the light, Γ_G is the internal gain, I_{ill} is the excitation power, d is the diameter of the ZnO−CdS wire, and l is the spacing between two electrodes. Remarkably, the calculated responsivity R of the present device is approximately 11 A W^{-1} at an intensity of 1.79 × 10^{-7} W/cm^2 of green light illumination (548 nm). This corresponds to an EQE of ~2.49 × 10^3% if the internal gain Γ_G is assumed to be 1. These values indicate, as for visible/UV light sensor, our device based on single ZnO−CdS wire exhibits ultrahigh responsivity R and EQE as well as wide spectral sensitivity (11 A W^{-1}, 2.49 × 10^3%, 548 nm, at 2 V bias), compared with individual ZnSe-nanobelt-based blue/UV-light sensor (0.12 A W^{-1}, 37.2%, 400 nm, at 30 V bias).[8] Besides, the decrease of the responsivity with high light intensities could be ascribed to the hole-trapping saturation and the Schottky barrier being transparent at high light intensity, as has also been observed from ZnO nanowire-based UV light photodetectors.[10]

In addition to the good sensitivity to green light, the ZnO−CdS wire-based photodetector also exhibits excellent response to UV light. Supporting Information, Figure S2 displays the performance of the device at wavelength of 372 nm. As expected, the responsivity R shows a notable increase by nearly 1 order of magnitude when the device is illuminated by 372 nm UV light, which is evident from the comparison of Figure 2d and Supporting Information, Figure S2d in the scale of the vertical axis. This enhancement should be ascribed to the coupling effect of the ZnO core and CdS shell. Since the excitation energy of the UV light (~3.34 eV, 372 nm) is larger than the band gap of CdS (~2.4 eV) and ZnO (~3.3 eV), electron−hole pairs can be generated both in the core and shell parts of the wire, which results in the increased amount of photocarriers. Consequently, the performance of the ZnO−CdS wire photodetector is significantly optimized compared to that of pure CdS or ZnO nanostructures by combining the high UV and visible light sensitivity, justifying the effective utilization of the present ZnO−CdS wire as the UV/visible light photodetector.

As described in our previous work, the internal piezoelectric field formed inside ZnO can tune the charge transport/separation process at the contact and thus optimize the photoresponse of a single ZnO wire.[10] To investigate the effects of the piezopotential on the performance of our photodetector (device #2), *I*−*V* characteristics of a single ZnO−CdS wire under a variety of compressive and tensile strain were measured under illumination of green light (548 nm, 1.43 × 10^{-3} W/cm^2), as shown in Figure 3a. The asymmetric *I*−*V* curves show excellent rectification behavior under all straining conditions and indicate two unequal back-to-back Schottky barriers at contacts, with Schottky barrier height (SBH) at the drain side (ϕ_d) being much higher than that at the source side (ϕ_s). In positive bias range, the photocurrent response of the device increased and decreased under compressive and tensile strain, respectively. The *I*−*V* curves could be recovered as the strains were released, and the extensive study indicates that the *I*−*V* behavior is introduced by strain rather than poor or unstable contact.

As is well studied, the Schottky barrier at the interface of a metal and semiconductor is an important factor in determining electrical transport properties of the metal−semiconductor−metal (M−S−M) structure. To understand the changes of *I*−*V* curves with strains in Figure 3a, we consider the current transport with illumination to be described by a relationship based on the thermionic emission−diffusion theory for $V \gg 3kT/q \approx 77$ mV,[22−24] thus the changes of SBH $\Delta\phi_s$ (at 2.0 V, black curve) and $\Delta\phi_d$ (at −2.0 V, red curve) with strain are calculated by[25,26]

$$\Delta\phi_B \sim -kT \ln[I(\varepsilon_{zz})/I(0)] \quad (3)$$

where ϕ_B is the SBH, k is the Boltzmann constant, $I(\varepsilon_{zz})$ and $I(0)$ are the current measured through the ZnO−CdS wire at a fixed bias V with and without being

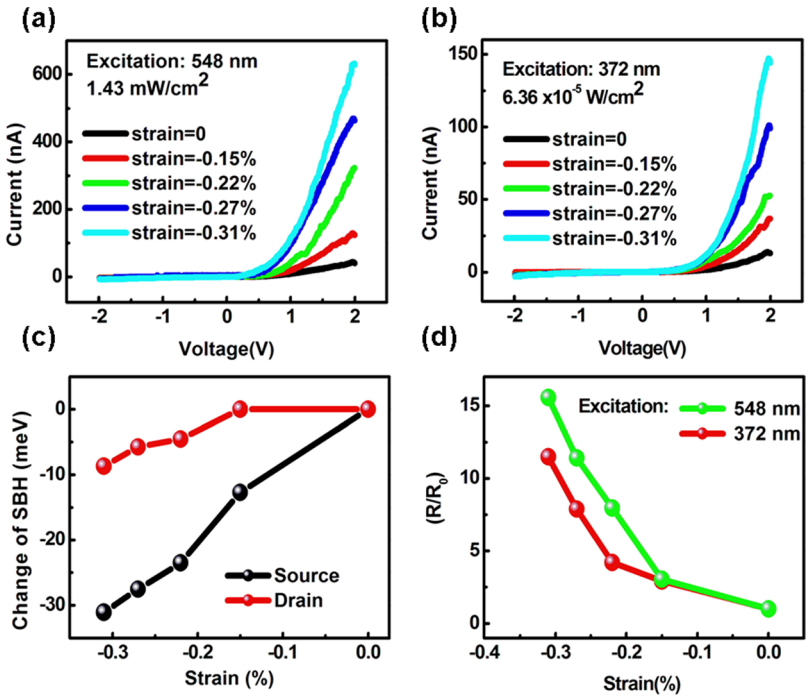

Figure 4. (a,b) Typical *I*−*V* characteristics of a single ZnO−CdS wire-based device under different compressive strains, excited by green light centered at 548 nm and UV light centered at 372 nm. (c) The derived change in SBH as a function of compressive strains using the thermionic emission−diffusion model. Black curve and red curve are the SBH change for source contact and drain contact at a source−drain bias of *V* = 2 and −2 V, respectively. (d) The change of responsivity under compressive strains, excited by green light centered at 548 nm and UV light centered at 372 nm; R_0 is set as responsivity under zero strain.

strained, respectively. It has been reported that the SBH shifts under strain are attributed to a combination of band structure and piezoelectric effect.[23,25] The band structure change (*e.g.*, the piezoresistive effect and parasitic capacitance effect) is a nonpolar effect on the electric transport; while the piezotronic effect is a polarized effect using the piezopotential as a "gate" voltage to tune charge carrier transport at the semiconductor−metal contact.[27,28] If we ignore the piezoresistive effect and use the experimental observed *I*−*V* as the starting curve to derive the change in SBH (see eq 3), we get the results shown in Figure 3b, in which both the SBHs at the source and drain contacts were decreased step-by-step with application of a variable strain from 0.22% tensile to −0.31% compressing but at different slopes, indicating an asymmetric change of SBHs at the source and drain contacts, which is the piezotronic effect.

To illustrate the piezopotential effect on the performance of the photodetector upon visible/UV light, respectively, we measured compressive strain-dependent *I*−*V* characteristics of a single ZnO−CdS wire (device #3) under illumination of green light (548 nm, 1.43×10^{-3} W/cm^2) and UV light (372 nm, 6.36×10^{-5} W/cm^2), as shown in Figure 4. The absolute current of the photodetector at a positive bias of 2.0 V increased gradually from 40 to 632 nA under green light illumination, with application of a variable strain from 0% to −0.31% (Figure 4a). Meanwhile, the current increased from 12.9 to 144 nA under UV light illumination (Figure 4b). Figure 4c shows the changes of SBH $\Delta\phi_d$ (red curve) and $\Delta\phi_s$ (black curve) with strains at a bias of 2 V. The result indicates that both the SBHs at the source and drain contacts were decreased with increased compressive strains. The asymmetric decreasing tendency implies the participation of the piezopotential effect,[23,27] which agrees well with the results in Figure 3b. Figure 4d shows the responsivity of the photodetector under different compressive strains upon green light (green curve) and UV light (red curve) illumination, respectively. It is noticed that the responsivity of the present ZnO−CdS wire-based photodetector is significantly enhanced by more than 10 times compared to that of the unstrained wire, indicating the piezo-phototronic effect on the ZnO−CdS wire as visible/UV photodetector.

It is interesting to understand the piezopotential enhanced performance of a strained photodetector under illumination of visible light and UV light, respectively. Here we use a schematic diagram (Figure 5) to illustrate how piezoelectric polarization affects the SBHs at the source and drain contacts and current output of the device under illumination. Figure 5a displays the type-II band alignment of ZnO−CdS heterostructure.[29] When the ZnO−CdS wire is under the illumination of green (548 nm) light, photogenerated electrons are injected from the conduction band (CB) of the photoexcited CdS into the CB of ZnO, leading to a high concentration of electrons in the CB of ZnO. Meanwhile, with a large amount of electrons

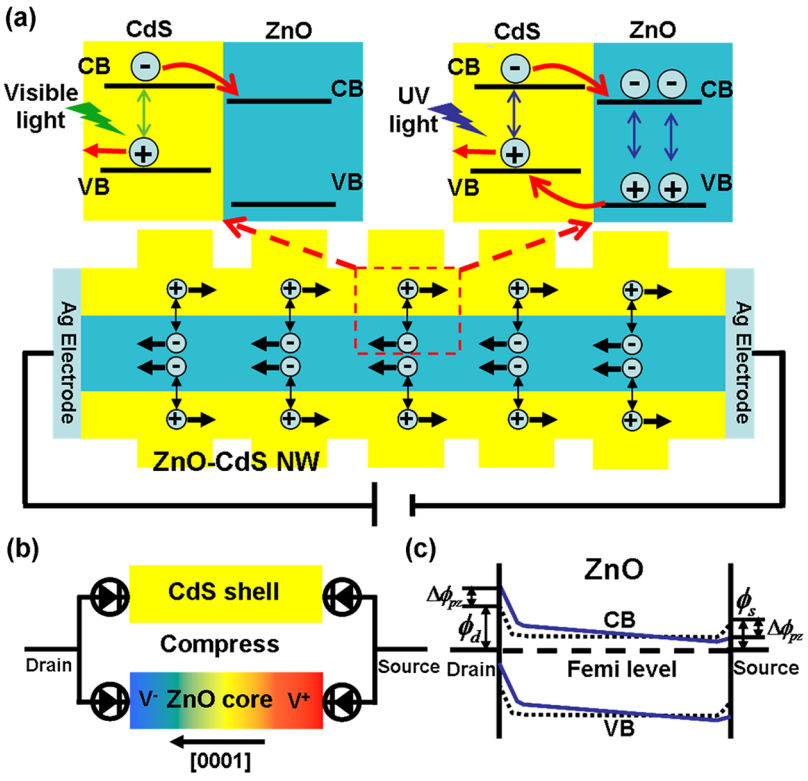

Figure 5. (a) Schematic diagram exhibiting the energy band structure, electron–hole pair separation, and transfer in the ZnO–CdS heterostructure under light illumination of green light centered at 548 nm and UV light centered at 372 nm. (b) The proposed sandwich model of the device, that is, two back-to-back Schottky diodes connected to a ZnO core and CdS shell, respectively, and simulation of the piezopotential distribution in the ZnO core under compressive strain. (c) Schematic energy band diagram illustrating the Schottky barriers at the source and drain contacts of an unstrained (dotted line) and compressive strained (solid line) ZnO wire, which shows the effect of switching the piezoelectric potential on the SBH.

moving into the ZnO, the high carrier mobility in the high-crystalline ZnO core makes it an effective channel for conducting electrons, while the holes are transported through CdS. The separation of the charge carrier types minimizes their recombination rate, thus, increasing the photocurrent. With considering the Schottky contact characteristics of the device, the conductance is mainly dominated by the local contacts.

Figure 5b shows the piezopotential distribution in a strained ZnO–CdS wire device under illumination. Since the *c*-axis (polarization direction) of the CdS NW array is approximately normal to direction of strain, only a band structure change (*e.g.*, piezoresistance) can be produced in the CdS shell along the length of the ZnO–CdS wire, which produces an equal effect to the SBHs at the source and drain contacts regardless of the polarity of the voltage. While, as the *c*-axis ([0001]) of ZnO NW is positioned in alignment with strain direction from the source to drain side, a piezopotential drop of approximately $V^+ - V^- = P_X L$ can be induced along the length of the ZnO core (where P_X is axial polarization and L is the length of the ZnO core). Thus, the piezopotential at the source and drain sides can be qualitatively described as V^+ and V^-, which are of the same magnitude but opposite in sign. As shown in Figure 5c, with the piezopotential modulations to the SBH denoted by $\Delta\phi_{pz}$, the drain has a negative piezopotential (V_p^-) leading to a increased SBH ($\phi_d + \Delta\phi_{pz}$), and the source has a positive piezopotential (V_p^+) leading to a decreased SBH ($\phi_s - \Delta\phi_{pz}$). Therefore, based on the strain induced piezopotential, an asymmetric change of SBHs at two contacts is introduced, which is just what we observed experimentally in Figures 3b and 4c. According to a previous report,[30] when a positive bias voltage V is applied at the drain side, the voltage drop occurs mainly at the reversely biased Schottky barrier ϕ_s at the source side. Consequently, the piezopotential induced decrease of SBH ($\phi_s - \Delta\phi_{pz}$) at the source side allows an significant increase of photocurrent and thus the photon responsivity.

Once the photodetector is under the illumination of UV light, electron–hole pairs can be generated in the ZnO NW core and CdS NW array shell, and the performance of the photodetector can be also enhanced by the strain-induced piezoelectric effect.

CONCLUSIONS

In summary, we first fabricated a novel ZnO–CdS micro/nanowire with the CdS NW array as the shell and a ZnO micro/nanowire as the core. Based on a single ZnO–CdS wire, we developed a photodetector exhibiting an excellent response on the wide-range visible/UV

light (372−548 nm). The photocurrent and sensitivity of the ZnO−CdS wire photodetector is 10^3 times higher than that of CdS nanoribbon, and the responsivity (11 A W^{-1}, 548 nm, at 2 V bias) is nearly 100 times higher than that of ZnSe-nanobelt-based blue/UV-light sensor (0.12 A W^{-1}, 400 nm, at 30 V bias). Moreover, the performance of the ZnO−CdS wire photodetector upon illumination of visible and UV light can be both further enhanced for more than 10 times with the participation of the piezo-phototronic effect when the device is subjected to a −0.31% compressive strain. This investigation extends the application of the piezo-phototronic effect in a wide spectrum photon detector.

EXPERIMENTAL SECTION

ZnO−CdS micro/nanowires were synthesized *via* a two-step process. First, ZnO micro/nanowires were synthesized by a high-temperature thermal evaporation process as described in our previous work.[13] Then, the CdS NW array was grown on ZnO micro/nanowire by hydrothermal method. Briefly, 1 mmol Cadmium nitrate ($Cd(NO_3)_2 \cdot 4H_2O$) and 3 mmol Thiourea (CH_4N_2S) were added to a given amount (80 mL) of distilled water. ZnO micro/nanowires were subsequently added to the result solution and the mixture was transferred into a Teflon-lined stainless autoclave (25 mL capacity). The autoclave was sealed and maintained at 200 °C for 12 h. After the system cooled down, the product was collected and vacuum-dried. The detailed microscopic structures of the precursor ZnO wires and the final ZnO−CdS wire products were characterized by TEM [JEOL 100CX at 100 kV, JEOL 4000EX at 400 kV, TF30 at 300 kV].

The device was fabricated following the method described in the literature.[10,11] In brief, two ends of a single ZnO−CdS wire were fixed on a PS substrate (typical length of ~3 cm, width of ~1 cm, and thickness of 0.5 mm) tightly by silver pastes which serviced as the source and drain electrodes. Then a thin layer of polydimethylsiloxane (PDMS) was utilized to package the device and make it optically transparent, flexible, and robust under repeated mechanical strains. (see Supporting Information, Figure S1). One end of the device was affixed on a 3D stage with movement resolution of 1 μm, which kept the device in focus under a microscope during the measurement process. Another 3D stage connecting to the free end of the device was used to produce a compressive or tensile strain on the substrate. The device was monitored by a Nikon Eclipse Ti inverted microscope system and excited by monochromatic UV light (centered at 372 nm) and green light (centered at 548 nm) with a Nikon Intensilight C-HGFIE lamp as the source. The optical power density illuminated on the device was varied by means of neutral density filters and determined by a thermopile power meter (Newport 818P-001-12). Meanwhile the *I*−*V* characteristics of the device were recorded by Keithley 487 picoammeter/voltage source in conjunction with a GPIB controller (National Instruments GPIB-USB-HS, NI 488.2).

Conflict of Interest: The authors declare no competing financial interest.

Acknowledgment. Research was supported by Airforce, MURI, U.S. Department of Energy, Office of Basic Energy Sciences (DE-FG02-07ER46394), NSF (CMMI 0403671), the Knowledge Innovation Program of the Chinese Academy of Sciences (KJCX2-YW-M13), National Nature Science Foundation of China (No. 21275018) and the 111 Project in China (B07012). Thanks are extended to Qing Yang, Ying Liu, Jianjun Chen, Guang Zhu, Caofeng Pan, Simiao Niu and Lin Dong for technical assistance.

Supporting Information Available: (1) Schematic diagram and optical microscopy image of a ZnO−CdS wire-based photodetector, schematic diagram of the measurement system; (2) performance of single ZnO−CdS wire-based photodetector under illumination of UV light centered at 372 nm. This material is available free of charge *via* the Internet at http://pubs.acs.org.

REFERENCES AND NOTES

1. Lieber, C. M.; Wang, Z. L. Functional Nanowires. *MRS Bull.* **2007**, *32*, 99–104.
2. Liu, S.; Ye, J. F.; Cao, Y.; Shen, Q.; Liu, Z. F.; Qi, L. M.; Guo, X. F. Tunable Hybrid Photodetectors with Superhigh Responsivity. *Small* **2009**, *5*, 2371–237.
3. Lao, C. S.; Park, M. C.; Kuang, Q.; Deng, Y. L.; Sood, A. K.; Polla, D. L.; Wang, Z. L. Giant Enhancement in UV Response of ZnO Nanobelts by Polymer Surface-Functionalization. *J. Am. Chem. Soc.* **2007**, *129*, 12096–12097.
4. Soci, C.; Zhang, A.; Xiang, B.; Dayeh, S. A.; Aplin, D. P. R.; Park, J.; Bao, X. Y.; Lo, Y. H.; Wang, D. ZnO Nanowire UV Photodetectors with High Internal Gain. *Nano Lett.* **2007**, *7*, 1003–1009.
5. Fang, X. S.; Bando, Y.; Liao, M. Y.; Gautam, U. K.; Zhi, C. Y.; Dierre, B.; Liu, B. D.; Zhai, T. Y.; Sekiguchi, T.; Koide, Y.; *et al.* Single-Crystalline ZnS Nanobelts as Ultraviolet-Light Sensors. *Adv. Mater.* **2009**, *21*, 2034–203.
6. Wei, T. Y.; Huang, C. T.; Hansen, B. J.; Lin, Y. F.; Chen, L. J.; Lu, S. Y.; Wang, Z. L. Large Enhancement in Photon Detection Sensitivity *via* Schottky-Gated CdS Nanowire Nanosensors. *Appl. Phys. Lett.* **2010**, *96*, 013508.
7. Kung, S. C.; van der, W. E. Veer; Yang, F.; Donavan, K. C.; Penner, R. M. 20 μs Photocurrent Response from Lithographically Patterned Nanocrystalline Cadmium Selenide Nanowires. *Nano Lett.* **2010**, *10*, 1481–1485.
8. Fang, X. S.; Xiong, S. L.; Zhai, T. Y.; Bando, Y.; Liao, M. Y.; Gautam, U. K.; Koide, Y. S.; Zhang, X. G.; Qian, Y. T.; *et al.* High-Performance Blue/Ultraviolet-Light-Sensitive ZnSe-Nanobelt Photodetectors. *Adv. Mater.* **2009**, *21*, 5016–5021.
9. Wang, Z. L. Self-Powered Nanosensors and Nanosystems. *Adv. Mater.* **2012**, *24*, 279.
10. Yang, Q.; Guo, X.; Wang, W. H.; Zhang, Y.; Xu, S.; Lien, D. H.; Wang, Z. L. Enhancing Sensitivity of a Single ZnO Micro-/Nanowire Photodetector by Piezo-phototronic Effect. *ACS Nano* **2010**, *4*, 6285–6291.
11. Liu, Y.; Yang, Q.; Zhang, Y.; Yang, Z. Y.; Wang, Z. L. Nanowire Piezo-phototronic Photodetector: Theory and Experimental Design. *Adv. Mater.* **2012**, *24*, 1410–1417.
12. Wang, Z. L. Progress in Piezotronics and Piezo-phototronics. *Adv. Mater.* **2012**, *24*, 4632–4646.
13. Pan, Z. W.; Dai, Z. R.; Wang, Z. L. Nanobelts of Semiconducting Oxides. *Science* **2001**, *291*, 1947–1949.
14. Jie, J. S.; Zhang, W. J.; Jiang, Y.; Meng, X. M.; Li, Y. Q.; Lee, S. T. Photoconductive Characteristics of Single-Crystal CdS Nanoribbons. *Nano Lett.* **2006**, *6*, 1887–1892.
15. Heo, K.; Lee, H.; Park, Y.; Park, J.; Lim, H. J.; Yoon, D.; Lee, C.; Kim, M.; Cheong, H.; Park, J.; *et al.* Aligned Networks of Cadmium Sulfide Nanowires for Highly Flexible Photodetectors with Improved Photoconductive Responses. *J. Mater. Chem.* **2012**, *22*, 2173–2179.
16. Muskens, O. L.; Rivas, J. G.; Algra, R. E.; Bakkers, E. P. A. M.; Lagendijk, A. Design of Light Scattering in Nanowire Materials for Photovoltaic Applications. *Nano Lett.* **2008**, *8*, 2638–2642.
17. Hu, L.; Chen, G. Analysis of Optical Absorption in Silicon Nanowire Arrays for Photovoltaic Applications. *Nano Lett.* **2007**, *7*, 3249–3252.
18. Tak, Y.; Hong, S. J.; Leeb, J. S.; Yong, K. Fabrication of ZnO/CdS Core/Shell Nanowire Arrays for Efficient Solar Energy Conversion. *J. Mater. Chem.* **2009**, *19*, 5945–5951.

19. Xu, F.; Yuan, Y. F.; Han, H. J.; Wu, D. P.; Gao, Z. Y.; Jiang, K. Synthesis of ZnO/CdS Hierarchical Heterostructure with Enhanced Photocatalytic Efficiency under Nature Sunlight. *CrystEngComm* **2012**, *14*, 3615–3622.
20. Hu, L. F.; Yan, J.; Liao, M. Y.; Xiang, H. J.; Gong, X. G.; Zhang, L. D.; Fang, X. S. An Optimized Ultraviolet—A Light Photodetector with Wide-Range Photoresponse Based on ZnS/ZnO Biaxial Nanobelt. *Adv. Mater.* **2012**, *24*, 2305–2309.
21. Konstantatos, G.; Sargent, E. H. Nanostructured Materials for Photon Detection. *Nat. Nanotechnol.* **2010**, *5*, 391–400.
22. Sze, S. M. *Physics of Semiconductor Devices*; Wiley: New York, 1981.
23. Ki-Woong Chung, Z. W.; Costa, J. C.; Williamson, F.; Ruden, P. P.; Nathan, M. I. Barrier Height Change in GaAs Schottky Diodes Induced by Piezoelectric Effect. *Appl. Phys. Lett.* **1991**, *59*, 1191–1193.
24. Shan, W.; Li, M. F.; Yu, P. Y.; Hansen, W. L.; Walukiewicz, W. Pressure-Dependence of Schottky-Barrier Height at the Pt/GaAs Interface. *Appl. Phys. Lett.* **1988**, *53*, 974–976.
25. Zhou, J.; Fei, P.; Gu, Y. D.; Mai, W. J.; Gao, Y. F.; Yang, R.; Bao, G.; Wang, Z. L. Piezoelectric-Potential-Controlled Polarity-Reversible Schottky Diodes and Switches of ZnO Wires. *Nano Lett.* **2008**, *8*, 3973–3977.
26. Zhou, J.; Gu, Y. D.; Fei, P.; Mai, W. J.; Gao, Y. F.; Yang, R. S.; Bao, G.; Wang, Z. L. Flexible Piezotronic Strain Sensor. *Nano Lett.* **2008**, *8*, 3035–3040.
27. Yu, R. M.; Dong, L.; Pan, C. F.; Niu, S. M.; Liu, H. F.; Liu, W.; Chua, S. J.; Chi, D. Z.; Wang, Z. L. Piezotronic Effect on the Transport Properties of GaN Nanobelts for Active Flexible Electronics. *Adv. Mater.* **2012**, *24*, 3532–3537.
28. Zhang, Y.; Hu, Y. F.; Xiang, S.; Wang, Z. L. Effects of Piezopotential Spatial Distribution on Local Contact Dictated Transport Property of ZnO Micro/Nanowires. *Appl. Phys. Lett.* **2010**, *97*, 033509.
29. Xu, Y.; Schoonen, M. M. A. The Absolute Energy Positions of Conduction and Valence Bands of Selected Semiconducting Minerals. *Am. Mineral.* **2000**, *85*, 543–556.
30. Fan, Z. Y.; Lu, J. G. Electrical Properties of ZnO Nanowire Field Effect Transistors Characterized with Scanning Probes. *Appl. Phys. Lett.* **2005**, *86*, 032111.